OXFORD

ENDOCRINE SOCIETY

Mapping Pregnancy-dependent Sulfhydrome Unfolds Diverse Functions of Protein Sulfhydration in Human Uterine Artery

Jin Bai,[1] Fenglong Jiao,[2] Alejandra Garcia Salmeron,[1] Shi Xu,[3] Ming Xian,[3] Lan Huang,[2] and Dong-bao Chen[1] (ORCID)

[1]Department of Obstetrics and Gynecology, University of California, Irvine, CA 92697, USA
[2]Department of Physiology and Biophysics, University of California, Irvine, CA 92697, USA
[3]Department of Chemistry, Brown University, Providence, RI 02912, USA

Correspondence: Dong-bao Chen, PhD, Department of Obstetrics and Gynecology, University of California Irvine, 140 Medical Surge 1, Irvine, CA 92697.
Email: dongbaoc@hs.uci.edu.

Abstract

Uterine artery (UA) hydrogen sulfide (H_2S) production is augmented in pregnancy and, on stimulation by systemic/local vasodilators, contributes to pregnancy-dependent uterine vasodilation; however, how H_2S exploits this role is largely unknown. S-sulfhydration converts free thiols to persulfides at reactive cysteine(s) on targeted proteins to affect the entire proteome posttranslationally, representing the main route for H_2S to elicit its function. Here, we used Tag-Switch to quantify changes in sulfhydrated (SSH-) proteins (ie, sulfhydrome) in H_2S-treated nonpregnant and pregnant human UA. We further used the low-pH quantitative thiol reactivity profiling platform by which paired sulfhydromes were subjected to liquid chromatography tandem mass spectrometry–based peptide sequencing to generate site (cysteine)-specific pregnancy-dependent H_2S-responsive human UA sulfhydrome. Total levels of sulfhydrated proteins were significantly greater in pregnant vs nonpregnant human UA and further stimulated by treatment with sodium hydrosulfide. We identified a total of 360 and 1671 SSH-peptides from 480 and 1186 SSH-proteins in untreated and sodium hydrosulfide–treated human UA, respectively. Bioinformatics analyses identified pregnancy-dependent H_2S-responsive human UA SSH peptides/proteins, which were categorized to various molecular functions, pathways, and biological processes, especially vascular smooth muscle contraction/relaxation. Pregnancy-dependent changes in these proteins were rectified by immunoblotting of the Tag-Switch labeled SSH proteins. Low-pH quantitative thiol reactivity profiling failed to identify low abundance SSH proteins such as K_{ATP} channels in human UA; however, immunoblotting of Tag-Switch–labeled SSH proteins identified pregnancy-dependent upregulation of SSH-K_{ATP} channels without altering their total proteins. Thus, comprehensive analyses of human UA sulfhydromes influenced by endogenous and exogenous H_2S inform novel roles of protein sulfhydration in uterine hemodynamics regulation.

Key Words: uterine artery, H_2S signaling, functional proteomics, sulfhydration, pregnancy

Abbreviations: ACTN1, α-actinin-1; ALB, albumin; BGN, biglycan; BK_{Ca}, Ca^{2+}-activated voltage-dependent potassium; CBS, cystathionine β-synthase; cGMP, cyclic GMP; COL4A1, collagen type IV alpha 1 chain; CSE, cystathionine γ-lyase; CSRP1, cysteine and glycine-rich protein 1; CSRP2, cysteine and glycine-rich protein 2; DCN, decorin; DRSP, differentially regulated sulfhydrated protein; DTT, dithiothreitol; FGB, fibrinogen β chain; FLNA, filamin A; GO, gene ontology; H_2S, hydrogen sulfide; HBB, hemoglobin subunit beta; IPM, iodo-N-(prop-2-yn-1-yl) acetamide; K_{ATP}, ATP-sensitive potassium; KEGG, Kyoto Encyclopedia of Genes and Genomes; LC-MS/MS, liquid chromatography tandem mass spectrometry; LDHA, lactate dehydrogenase A; low-pH QTRP, low-pH quantitative thiol reactivity proteomics; MSBT-A, methylsulfonyl-benzothiazole; MYH, myosin; NaHS, sodium hydrosulfide; NaOAC, sodium acetate; NO, nitric oxide; NP, nonpregnant; P, pregnant; PDE5A, phosphodiesterase type 5; PTM, posttranslational modification; QPers-SID, quantitative persulfide site identification; RT, room temperature; SNO, S-nitrosylation; -SH, free thiol; -SSH, hydropersulfide moiety; SUR2B, sulfonylurea receptor; UA, uterine artery; VEGF, vascular endothelial growth factor; VIM, vimentin.

Normal pregnancy is associated with gestation age-dependent rises in uterine blood flow mandatory to the delivery of maternal nutrients and oxygen to the fetus and the exhaust of respiratory gases (CO_2) and metabolic wastes of the fetus (1, 2). Insufficient rise in uterine blood flow during pregnancy results in placental ischemia/hypoxia, representing a major pathology underlying numerous pregnancy disorders including preeclampsia, fetal growth restriction, and preterm birth (3, 4). These diseases increase maternal and fetal morbidity and mortality during pregnancy and harm both the mother and her child's long-term health trajectory in later life (5). Uterine hemodynamics is regulated by incompletely understood complex mechanisms, but orchestrated vasodilators produced by uterine artery (UA) locally are recognized to be the dominating forces that drive uterine blood flow to rise. Endothelium-derived nitric oxide (NO) is the most studied UA vasodilator and mediates the convergence of other systemic/local uterine vasodilatory signals, including elevated endogenous estrogens and vascular endothelial growth factor (VEGF) (6). Clinical trials targeting NO-mediated mechanisms in preeclampsia and fetal growth restriction have achieved no to little success (7, 8), suggesting mechanisms in addition to NO to be involved in mediating uterine hemodynamics regulation.

Endogenous hydrogen sulfide (H_2S) is mainly produced by L-cysteine metabolizing enzymes cystathionine β-synthase (CBS) and cystathionine γ-lyase (CSE). H_2S possesses potent proangiogenic, vasodilatory, anti-inflammatory, and antioxidant effects at physiological levels in the low micromolar range (9, 10). UA endothelium and smooth muscle H_2S production is stimulated via selective CBS upregulation by exogenous estrogens and is associated with elevated endogenous estrogens during ovine and human pregnancy in vivo (11-13). Estrogens and VEGF also stimulate human UA endothelial cell H_2S production via CBS upregulation in vitro (14, 15). H_2S stimulates pregnancy-dependent relaxation of pressurized rat and human UA rings in vitro (13, 16). Thus, CBS-H_2S has emerged as a novel pathway alongside NO to regulate uterine hemodynamics, although how H_2S exploits this role is largely unknown.

H_2S is a small cyanide that can freely cross cell membranes, and its reducing capacity enables it to react with many molecules (10). H_2S signaling is complex and incompletely understood, but regulating protein function posttranslationally via *S*-sulfhydration directly is recognized to be the major route for H_2S to exert its biological function. *S*-sulfhydration generates a hydropersulfide moiety (-SSH) from free thiols (-SH) at reactive cysteine(s) on targeted proteins, resulting in increased reactivity of modified cysteines because of greater nucleophilicity of -SSH vs -SH (17, 18). Because cysteine is an essential amino acid, sulfhydration can potentially change the entire proteome. Sulfhydration occurs in up to 25% of all proteins (19), thus inevitably participating in regulating diverse biological processes including Ca2+ signaling, apoptosis, redox signaling, angiogenesis, vascular tone, and cardioprotection (20, 21). Dysregulated protein sulfhydration has been reported in numerous diseases, including preeclampsia (22-26), highlighting the need of high throughput identification of sulfhydrated proteins (eg, sulfhydrome) in the proteome to comprehend the importance of sulfhydration in diverse biological processes in physiological and pathophysiological settings.

The S-SH bond is intrinsically unstable and shares similar reactivity to other sulfur species, especially SH (10), making it challenging to detect sulfhydrated proteins in complex biological samples. Most methods for detecting sulfhydrated proteins are indirect, involving incorporating a stable modification to label S-SH with a tag so that it can be readily determined. The Tag-Switch method was invented to specifically label SSH groups, in which SSH and SH groups are first blocked by methylsulfonyl-benzothiazole (MSBT-A) and then SSH is selectively labeled by a cyanoacetate-based reagent CN-biotin because SSH possesses enhanced reactivity to nucleophilic attack by CN-biotin, whereas SH adducts are thioethers that do not react with nucleophiles (27). Biotinylated sulfhydrated proteins can then be identified by peptide sequencing using liquid chromatography tandem mass spectrometry (LC-MS/MS) (28). More recently, a chemoproteomic platform called low-pH quantitative thiol reactivity profiling (low-pH QTRP) enables direct site-specific mapping and proteomic profiling of SSH and SH groups simultaneously (29), in which sulfhydrated proteins are preferentially labeled because of an approximate 4 U lower pKa of a persulfide than that of a free thiol (30).

Here, we used Tag-Switch to quantify sulfhydrated proteins in H_2S-treated nonpregnant (NP) and pregnant (P) human UA sulfhydromes; we then further analyzed them by the low-pH QTRP platform to generate site (cysteine)-specific pregnancy-dependent H_2S-responsive human UA sulfhydrome. We also developed bioinformatics tools to analyze UA sulfhydromes to identify the biological functions and pathways and the interactomes of the differentially regulated sulfhydrated proteins (DRSPs). Our study informs novel diverse roles of protein sulfhydration in uterine hemodynamics regulation.

Materials and Methods

Chemicals and Antibodies

MSBT-A and CN-biotin were synthesized as described previously (27). Sequencing-grade trypsin was from Promega (Madison, WI). Fetal bovine serum, DMEM medium, penicillin-streptomycin, dithiothreitol (DTT), HPLC-grade water, formic acid, acetonitrile, and methanol were from Thermo Fisher Scientific (Waltham, MA). Electrophilic thiol-reactive probe iodo-N-(prop-2-yn-1-yl) acetamide (IPM), light- and heavy-labeled UV-cleavable azido-UV-cleavable-biotin reagents were from KeraFast (Boston, MA). Streptavidin sepharose beads were from GE (Chicago, IL). Anti-biotin antibody was from Cell Signaling (RRID: AB_10696897, Beverly, MA). Anti-β-actin antibody was from Ambion (RRID: AB_437394, Austin, TX). Antibodies of α-actinin-1 (ACTN1, RRID: AB_626633), vimentin (VIM, RRID: AB_628437), myosin 11 (MYH11, RRID: AB_1126447), talin 1 (TLN1, RRID: AB_2303406), vinculin (VCL, RRID: AB_1131294), and cofilin 1 (CFL1, RRID: AB_11150468) were from Santa Cruz (Santa Cruz, CA). Kir6.1 antibody was from Biorbyt (RRID: AB_2940873, Durham, NC). Sulfonylurea receptor (SUR2B) antibody was from Sigma (RRID: AB_2940874, Burlington, MA). Secondary antibodies goat anti-mouse IgG (H + L) horseradish peroxidase (RRID: AB_1185566) and goat anti-rabbit IgG (H + L) horseradish peroxidase (RRID: AB_1185567) were from Invitrogen (Waltham, MA). Information on all antibodies is detailed in Supplementary Table S1 (31). All other chemicals unless specified were from Sigma (St. Louis, MO).

Human Subjects and UA Collection

Human UAs were collected with written consent from NP and P women (n = 3/group) undergoing hysterectomy at the University of California Irvine Medical Center, with ethical approval (HS #20139763) from the Institutional Review Board for Human Research, as described in our previous study (15). All subjects were not on steroid treatment. The 3 NP subjects were 2 premenopausal (aged 39 and 41 years) and 1 postmenopausal (aged 50 years) women and their uterus were removed because of fibroids with no other known complications. The three P subjects were aged 25, 27, and 30 years and their uterus were removed at gestation 34 to 36 weeks because of placenta accreta without other complications.

Tag-Switch and Immunoblotting

Tag-Switch was performed to specifically label sulfhydrated proteins as described previously (27). Briefly, hUA segments (~200 mg/sample) were treated with or without 0.3 mM sodium hydrosulfide (NaHS) in PBS at 37 °C for 30 minutes. Sodium hydrosulfide–treated P UA was also treated with 1-mM reducing agent DTT. The hUA segments were then minced, washed twice with ice-cold PBS, and lysed by 5 × 20s cycles of sonication in 200-μL HEN buffer (250 mM HEPES, 50 mM NaCl, 1 mM EDTA, 0.1 mM neocuproine, 1% NP-40) containing 1% SDS, 30 mM MSTB-A, and a

protease inhibitor cocktail (Roche, Switzerland, Basel) on ice. The lysates were incubated at 37 °C for 1 hour. Proteins were acetone-precipitated, resuspended in 60 μL HEN buffer containing 20-mM CN-biotin and 2.5% SDS, and then incubated at 37 °C for 1 hour. Excess CN-biotin was removed by passing the samples through Micro Bio-Spin P-6 gel columns (BioRad, Hercules, CA). An aliquot (15 μL) of each eluate was saved as the input mixed with nonreducing Laemmli buffer before heat denaturation. The rest of the eluates was mixed with streptavidin-coated magnetic beads (40 μL, Thermo Fisher) and incubated at 4 °C overnight with gentle rotation. The beads were washed with PBS twice, mixed with SDS sample buffer, and boiled at 95 °C for 5 minutes. The samples (purified biotinylated SSH proteins) were subjected to SDS-PAGE and immunoblotted with anti-biotin (1:10 000) and other antibodies listed in Supplementary Table S1 (31), as previously described (15). Parallel blots of the inputs with anti-β-actin were conducted to serve as loading controls. Band intensities of total SSH proteins were summed and normalized to β-actin as did levels of total proteins, whereas SSH protein was normalized to total protein, by using NIH ImageJ and presented as fold of corresponding controls.

Low-pH QTRP Proteomics

Human UA sulfhydromes were analyzed by using the low-pH QTRP platform (30), with minor modifications as described here.

IPM-labeling SSH proteins and tryptic digestion: Human UA samples (200 mg/sample) were washed with ice-cold PBS and lysed by sonication on ice for 5 sets of 20-second pulses using a VirTis Virsonic 100 Ultrasonic Homogenizer/Sonicator at setting 3 with a 1/8-inch probe in low-pH buffer (50 mM sodium acetate [NaOAc], 1% Igepal, pH 5.0) supplemented with a protease inhibitor cocktail and catalase (200 U/mL). The lysates were incubated with or without 0.3 mM NaHS at 37 °C for 1 hour, followed by incubation with IPM probes (10 μM) in dark at room temperature (RT) for 1 hour. The samples were alkylated by iodoacetamide (mM) in the dark at RT for 30 minutes. Proteins were acetone-precipitated and resuspended to a final concentration of 1 mg/mL in 50-mM ammonium bicarbonate (pH 8.5).

IPM-labeled peptides were desalted with Sep-Pak tC18 1 cc Vac cartridges (Waters, Milford, MA) and dried under vacuum at 45 °C. The samples were reconstituted in 30% acetonitrile at pH 6. Equal amounts of NP and P UA samples were incubated in separate click chemical reactions with either 1 mM of light or heavy UV-cleavable azido-biotin, respectively, in a buffer containing 10 mM sodium ascorbate, 1 mM TBTA, and 10 mM CuSO$_4$, with rotation in the dark at RT for 2 hours, and then mixed. Samples were purified by stringent cation-exchange chromatography (The Nest Group, Ipswich, MA) as described previously (30) and captured by streptavidin-sepharose beads in the dark at RT for 2 hours. After sequential washing with streptavidin binding buffer (50 mM NaOAc, pH 4.5), washing buffer (50 mM NaOAc, 2 M NaCl, pH 4.5), and HPLC-grade water twice each to remove nonspecifically bound peptides. The beads were reconstituted in 25-mM ammonium bicarbonate for photo releasing in a glass tube by irradiation with 365-nm UV light at RT with stirring for 2 hours. After centrifugation (2000*g*, 4 minutes), supernatant was collected, vacuum-dried, and stored at −20 °C until LC-MS/MS analysis was performed.

Peptide sequencing by LC-MS/MS: Peptide sequencing was performed by LC-MS/MS using an UltiMate 3000 UHPLC (Thermo Fisher Scientific) coupled in-line with an Orbitrap Fusion Lumos MS (Thermo Fisher Scientific) using an ESI nanospray source. Mobile phase B was 0.1% formic acid in acetonitrile with a flow rate of 300 nL/minute. The digested peptides were separated over a 114-minute gradient from 4% to 25% mobile phase B (run time: 120 minutes/sample) on an Acclaim PepMap RSLC column (50 cm × 75 μm). Survey scans (MS) were acquired in Orbitrap (FT) with an Automated Gain Control target of 8E5, maximum injection time 50 ms, and dynamic exclusion of 30s across the scan range of 375 to 1800 m/z. MS/MS spectra were acquired in data-dependent acquisition mode at the top speed for 3 seconds per cycle. The Automated Gain Control target was set to 1E4 with maximum injection time of 35 ms. Ions were subjected to stepped-energy higher energy collision dissociation fragmentation at a normalized collision energy of 20 ± 5%.

Label-free quantification analysis: The acquired LC-MS/MS data files were analyzed by Maxquant (version 2.0.3.1), with the spectra searched against the UniProt Human database (updated on July 1, 2022). For peptide identification, mass tolerances were set at 20 ppm for initial precursor ions and 0.6 Da for fragmental ions. Two missed cleavages in tryptic digests and a maximum of 2 variable modifications including cysteine methionine oxidation and N-terminal acetylation were allowed. IPM_L and IPM_H for -SH and IPM_SSH_L or IPM_SSH_H for -SSH were added as additional variable modifications. The false discovery rate was set at 1% for filtering peptide identification.

Bioinformatics

The clusterProfiler package in R studio (32) was used to identify and visualize enriched pathways among sulfhydrated proteins. The "enrichGO" and "enrichMKEGG" functions were used to identify overrepresented pathways ($P < .01$) based on Gene Ontology (GO) and Kyoto Encyclopedia of Genes and Genomes (KEGG) modules, respectively. The "barplot" function was used to visualize orthogonal GO molecular function and biological process. The "browseKEGG" function in KEGG module database (https://www.genome.jp/kegg/module.html) was used to determine KEGG pathways. The pheatmap package (33) in R studio was used to construct a heatmap to demonstrate the relative intensity of SH and SSH peptides by z scores calculated by the equation: $z = \frac{(x-\mu)}{\sigma}$; in which x is abundance of taxonomic or functional profiles in each group, μ is mean value of abundances in all groups, and σ is SD of abundances. A volcano plot was created using P values and fold changes in disulfide peptide intensities in P over NP UA. DRSPs were defined for SSH peptide/proteins with $P < .05$ and a fold change <0.5 or >2 between 2 groups in P vs NP or treated vs untreated groups.

Putative Consensus Sequence Motif for SSH

According to sulfhydrated and unsulfhydrated peptides and proteins from hUA (current study), and those in mouse liver, heart, and brain tissues and human A549, A431, HEK293, MDA-MB-231, U2OS, and pancreatic cells (22, 30, 34), we used a linear sequence prediction algorithm visualized by pLogo (35) to analyze putative SSH vs SH cysteines in 13-amino acid consensus sequence motifs. The normal procedure for computing 1-tailed significance is to calculate area under desired side of a probability distribution, whereas this pLogo method determines over- and underrepresentations of appropriate sides of distribution by using logics and

cases. A continuous probability-based score generates the pLogo by making residue heights proportional to log odds of significances of over- vs underrepresentations. The amino acid frequencies observed in a set of proteins that are representative of the proteome, namely the proteomic background, were used to calculate *P* values based on the binomial probability of residue frequencies with the following formula:

$$\text{Residue height } (K, N, P) \propto -\log \frac{\Pr(k, \ \forall k \geq K|N, p)}{\Pr(k, \ \forall k \leq K|N, p)}.$$

P value was determined by background population, such that:

$$\Pr(k, \ \forall k \geq K|N, p) = \sum_{k=K}^{N} binomial(k, N, p)$$

$$\Pr(k, \ \forall k \leq K|N, p) = \sum_{k=0}^{K} binomial(k, N, p)$$

K is the actual number of residues of a particular type at a given position, *N* is total number of residues at a position, and *P* is the probability of the residue occurring at that position.

Based on statistical significance $P < .05$ and the number of the sequences, the log-odds of the binomial probability >3.68 was calculated as a threshold to predict a specific cysteine residing a 13 amino-acid motif to be a putative sulfhydration site.

Statistical Analysis

Each experiment was repeated at least 3 times using samples from different subjects. Data were presented as means ± standard error of the mean and analyzed by 1-way ANOVA, followed by the Newman Keuls test for multiple comparisons using Sigmaplot 14 (Systat Software Inc.). Student *t*-test was used to compare 2 groups. $P < .05$ or lower was defined as statistically significant.

Results

Human UA Protein Sulfhydration—Effects of Pregnancy and Exogenous H₂S

Levels of total sulfhydrated proteins in P UA were 1.80 ± 0.28-fold greater ($P < .05$) than that in NP UA. Treatment

with NaHS increased total sulfhydrated proteins by 1.67 ± 0.17-fold ($P < .05$) in NP UA but did not affect sulfhydration in P UA. In addition, treatment with 1 mM DTT significantly reduced baseline total sulfhydrated proteins in P UA (Fig. 1).

Workflow of Low-pH QTRP

The low-pH QTRP platform was designed to directly analyze paired proteomes to identify SSH and SH peptides simultaneously in a single run, as summarized in a workflow (Fig. 2). In this study, we paired proteomes of equal amounts of NP and P UAs, and each was treated with and without 0.3 mM NaHS. IPM labeling was performed in buffers at pH 5.0. The probe-labeled proteomes were alkylated directly with iodoacetamide and digested into tryptic peptides. The IPM-labeled peptides in paired proteomes were conjugated with either light or heavy Az-UV-biotin reagents via copper-catalyzed alkyne–azide cycloaddition separately, and then mixed. Biotinylated peptides from the paired proteomes were captured by streptavidin beads and photo-released for peptide sequencing by LC-MS/MS. Two types of probe-modified peptides including disulfide and thioether forms were used for mapping SSH and SH sites (cysteines), respectively (Fig. 2A). For example, we identified an IPM-modified disulfide peptide containing Cys796 in filamin A as shown by the characteristic isotopic envelopes in the representative MS1 spectrum. The ratio of the paired heavy and light peptides was calculated from the extracted ion chromatogram peaks as 1.99 E5/4.15 E4 (Fig. 2B). The fully annotated high-energy collisional dissociation-MS2 spectrum showed the amino acids (Fig. 2C).

Human UA Sulfhydromes—Effects of Pregnancy and Exogenous H₂S

By using low-pH QTRP analysis, we obtained a total of 2460 SH peptides and 360 SSH peptides in hUA as summed in Supplementary Table S2 (31). Among 2460 SH peptides, 1146 were found in both NP and P UAs, whereas 93 and 1221 were unique to NP and P UA, respectively. The SH peptides were mapped to a total of 1984 proteins including 756 found in both NP and P UAs, 375 unique to NP UA, and 853 unique to P UA. Among the 360 SSH peptides identified,
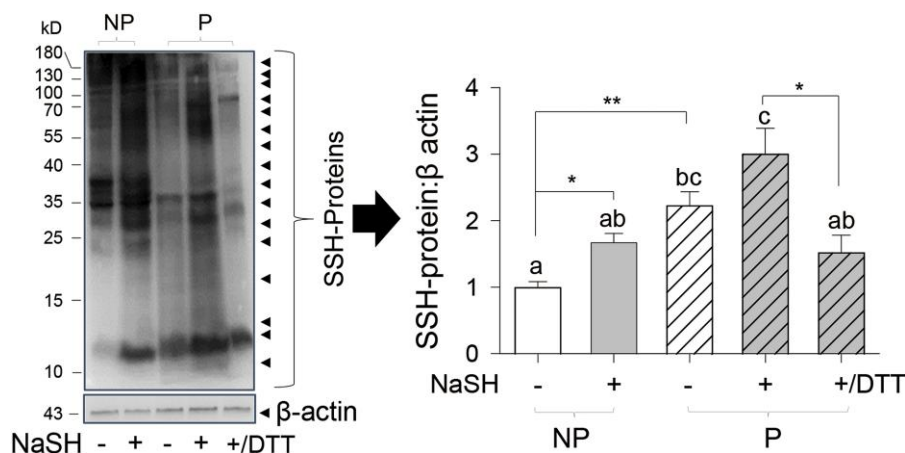

Figure 1. Human uterine artery (UA) protein sulfhydration: effects of pregnancy and exogenous H₂S. Human UA segments were treated with or without 0.3 mM NaHS or cotreated with 0.3 mM NaHS and 1 mM dithiothreitol (DTT). Human UA lysates were used for determining total SSH proteins. Representative blots of total SSH proteins and β-actin were shown. Data (mean ± standard error of the mean, n = 3) were presented as fold of controls. *$P < .05$, **$P < .01$ vs control. Bars with different letters differ significantly ($P < 0.05$).

45 were found in both NP and P UAs, whereas 157 and 158 were unique to NP and P UA, respectively (Fig. 3A, left). The 360 SSH peptides were mapped to a total of 408 SSH proteins because of a single SSH peptide originating from multiple proteins, including 45 in both NP and P UAs and 186 and 177 unique to NP and P UA, respectively (Fig. 3A, right).

Consistent with the finding showing NaHS stimulation of protein sulfhydration in NP UA (Fig. 1), NaHS treatment also stimulated significant shifts of the number of SH peptides to SSH peptides in NP UA; the total number of SH peptides reduced from 1239 to 208, but the total number of SSH peptides increased from 202 to 1047 on NaHS treatment (Supplementary Table S3 (31)). Similar shifts of total number of SH and SSH peptides also occurred in NaHS-treated P UA; the total number of SH peptides decreased from 2367 to 237, whereas the total numbers of SSH peptides increased from 203 to 1354 (Fig. 3A, left) on NaHS treatment. Accordingly, the total number of SH proteins decreased from 1984 to 365, whereas the total number of SSH proteins increased from 408 to 1218 on NaHS treatment in NP UA. Similar changes in SH vs SSH proteins also occurred in P UA with NaHS treatment; the total number of SH proteins decreased from 1609 to 258, whereas the total number of SSH proteins increased from 222 to 980 (Fig. 3A, right), although NaHS did not alter the total levels of sulfhydrated proteins in P UA (Fig. 1).

Pregnancy-dependent H_2S-responsive SSH-peptides

We then analyzed the SH peptides and SSH peptides in untreated and NaHS-treated NP and P UAs. The SH peptides and SSH peptides were depicted in a heatmap in which upregulated peptides are labeled in red and downregulated peptides are labeled in green (Fig. 4A). Most of the SH peptides were upregulated in untreated P vs NP UAs. Levels of detectable baseline SSH-peptides were either upregulated or downregulated in P vs NP UAs. In addition, the heatmap showed that treatment with NaHS dramatically changed the patterns of SH vs SSH peptides in NP and P UAs. Pregnancy upregulated most of the SSH peptides but downregulated only a few other SH peptides in UA (Fig. 4A).

We further analyzed the exogenous H_2S-responsive SSH peptides in NP vs P UAs. There were differentially regulated SSH peptides derived from SSH proteins that were identified in both NP and P UAs, including filamin A (FLNA), hemoglobin subunit beta (HBB), fibrinogen β chain (FGB), collagen type IV alpha 1 chain (COL4A1), myosin 9/10/11 (MYH 9/10/11), and cysteine and glycine-rich protein 1 (CSRP1). Some repeatedly detectable (n > 2) SSH peptides were derived from SSH proteins present in only NP UA, including albumin (ALB), destrin, VIM, biglycan (BGN), and decorin (DCN); whereas other detectable SSH peptides were derived from SSH proteins present in only P UA, including catalase, collagen type IV alpha 2 chain, tubulin alpha-4A chain. The heatmap showed that NaHS upregulated SSH peptides derived from FLNA, FGB, destrin, HBB, COL4A1, MYH 9/10/11, CSRP1, BGN, and DCN, but downregulated SSH peptides derived from ALB, FLNA, and BGN in NP UA. NaHS treatment upregulated SSH peptides from FLNA, FGB, HBB, MYH 9/10/11, catalase, and CSRP1 and downregulated some other SSH peptides from COL4A1, collagen type IV alpha 2 chain, tubulin alpha-4A chain, and MYH 9/10/11 in P UA.

These analyses also showed that some SSH proteins only generated 1 SSH peptide, indicative 1 specific SSH site in these SSH proteins such as SSH-VIM. Other SSH proteins generated multiple SSH peptides, suggesting that SSH can also occur on multiple sites in these proteins such as FLNA, BGN, and ALB, α-smooth muscle actin/ACTA1, TLN1, VCL, ACTN1, CFL1, and MYH11. In the latter case, levels of the SSH peptides from the same protein were found to be either all upregulated, unchanged, or regulated in opposite directions, in P vs NP or by NaHS treatment. For example, the SSH peptides derived from FLNA or BGN were either upregulated or downregulated but these from ALB were all downregulated in NP UA. FLNA generated different SSH peptides in NP vs P UA, showing SSH on different cysteines in pregnancy, although they were all upregulated by NaHS in P UA (Fig. 4B).

We plotted differentially regulated SSH peptides in NaHS-treated NP and P UAs in a volcano plot (Fig. 4C), using red dots showing upregulated SSH-peptides with fold change >2 and blue dots showing downregulated those with <0.5 fold. Most of the pregnancy-dependent H_2S-responsive SSH peptides are upregulated, including these derived from FLNA, MYH 9/10/11, mth938 domain-containing protein, raftlin 1, HBB, BGN, DCAN, versican core protein, and 60S ribosomal protein L12, as listed in Supplementary Table S3 (31). Only 2 SSH peptide derived from CSRP protein 2 (CSRP2) was found to be downregulated in pregnancy (Fig. 4C).

Prediction of Putative SSH Peptides

The flanking amino acid sequences of SSH cysteine from in vivo studies of human UA and mouse liver, brain, and heart (30) tissues and in vitro studies of human A549, A431, HEK293, MDA-MB-231, U2OS, and pancreatic cells (22, 30, 34) predicted a putative SSH peptide as KXXEEECE(K)VKIXK (Fig. 5A). The flanking amino acid sequences of unsulfhydrated cysteines predicted putative SH peptide as K(D)K(D)LDND(N)CDLKKKK (Fig. 5B). The acidic amino acid Glu (E) occurred frequently surrounding sulfhydrated cysteines at positions −1, −2, −3, and +1, whereas a basic amino acid Lys (K) only appeared at positions −6, +1, +3, and +6. Acidic amino acid Asp (D) was found nearby unsulfhydrated cysteines at positions −6, −5, −3, −1, and +1. A basic amino acid Lys (K) was highly overrepresented at positions −6, −5, +1, +3, +4, +5, and +6 (Fig. 5B).

Functional Analysis of Pregnancy-dependent H_2S-responsive Human UA SSH proteins

We further performed GO classifications to identify the biological functions, pathways, and the interactomes of protein sulfhydration in human UA. The DRSPs unique to NP UA were involved in various biological processes including metabolisms of nucleotides (eg, purine ribonucleotide, ribose phosphate, purine ribonucleotide triphosphate), axon development, ATP metabolism, protein folding, and negative regulation of protein procession linked to molecular functions including cadherin binding, actin filament binding, oxidoreductase activity, and cyclosporin A binding (Fig. 6A). Especially, the metabolisms of nucleotide-related biological processes were highly represented among the DRSPs unique to NP UA, including nucleoside diphosphate kinase 1 and 2, adenylate kinase, pyruvate kinase, signal transducer and activator of transcription 3, glyceraldehyde 3-phosphate dehydrogenase, ATP synthase subunit epsilon, mitochondrial (Supplementary Table S2) (31). The DRSPs unique to P UA were found to be involved in different biological
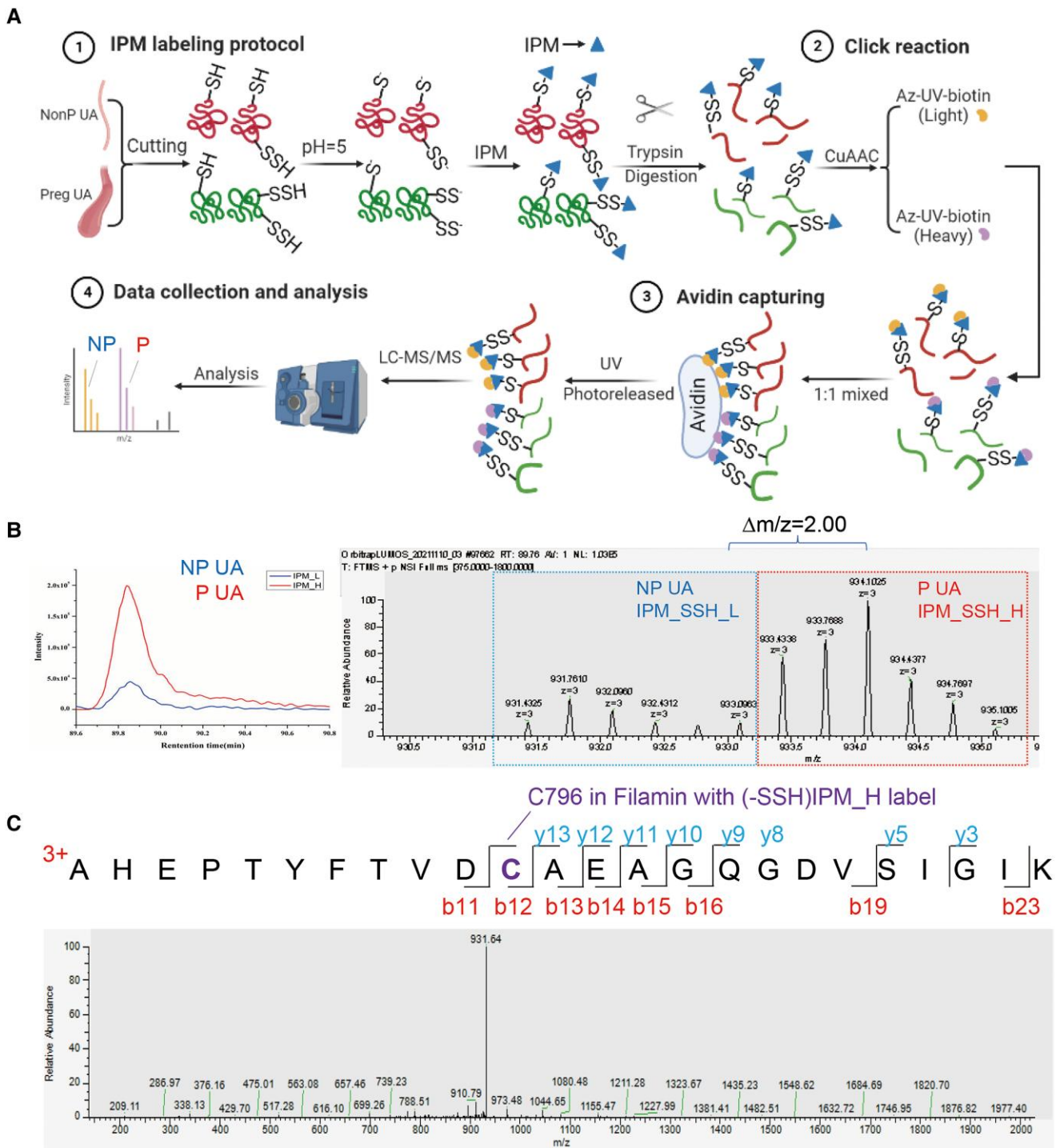
Figure 2. Low-pH quantitative thiol reactivity proteomics (low-pH QTRP) platform. (A) General workflow. Equal amounts of nonpregnant and pregnant human uterine arteries (UAs) were labeled with iodo-N-(prop-2-yn-1-yl) acetamide (IPM) directly in a buffer at pH 5.0, and then tryptically digested. The IPM-labeled peptides in paired proteomes were conjugated with either light or heavy Az-UV-biotin reagents via copper-catalyzed alkyne–azide cycloaddition (CuAAC) separately and then mixed. Biotinylated peptides from the paired proteomes were captured by streptavidin-coated beads and photo-released for peptide sequencing by LC-MS/MS. Two types of probe-modified peptides including SSH and SH forms for mapping SSH and SH sites (cysteines), respectively. (B) Quantification of Cys796-containing SSH-peptide of filamin A in human UA. MS1 spectrum of an IPM-tagged SSH-peptide containing filamin A C796. Triply charged monoisotopic precursors of light and heavy peptides are observed at m/z 932.0960 and 934.1025, respectively, with mass errors less than 10.0 ppm. Extracted-ion chromatogram (XIC) shows the profiles for the same light and heavy peptides. (C) Characterization of Cys796-containing SSH-peptide of filamin A. Fully annotated MS/MS spectra was applied to the light and heavy IPM-modified SSH peptide.

processes such as wounding healing, cellular responses to growth factor stimulus and hemostasis, blood coagulation, and fibrinolysis, which were linked to molecular functions including tubulin binding, microtubule binding, flavine adenine dinucleotide

binding, ECM binding, and epidermal growth factor receptor binding (Fig. 6B). The wound healing–related biological processes were highly represented among the DRSPs unique to P UA, including A disintegrin and metalloproteinase with
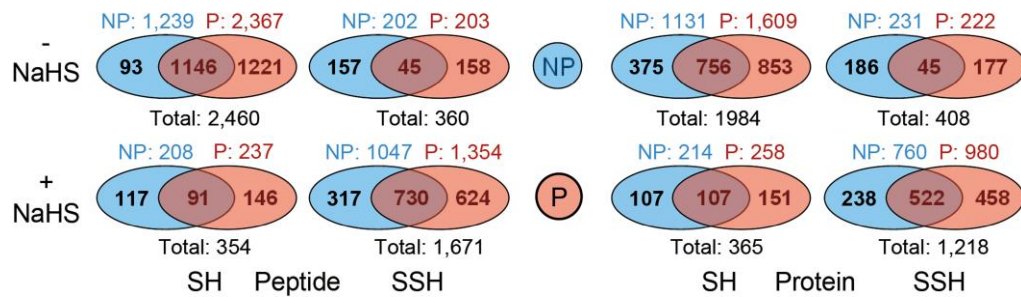
Figure 3. Summary of human uterine artery sulfhydromes. Venn diagram of SH peptides and SSH peptides (left) and SH-proteins and SSH-proteins (right) in nonpregnant (NP) and pregnant (P) human uterine arteries (UA) without (upper) or with (lower) NaHS treatment.

thrombospondin motifs 18, dual oxidase 1, ephrin type-B receptor 2, annexin 1, fibrinogen γ chain, peroxiredoxin 2, and F12 (Supplementary Table S2) (31). The H_2S-responsive DRSPs in NP UA were enriched in different biological processes, including actin filament organization, muscle system process, actomyosin structure organization, muscle cell development, and actin-filament sliding movement, which were linked to molecular functions of actin binding, ECM structural constitute, oxidoreductase activity, integrin binding, NAD binding, microfilament motor activity, and vinculin binding (Fig. 6C). Except for these in NP UA, the H_2S-responsive DRSPs in P UA also highlighted biological process of protein polymerization and molecular functions of ECM binding and laminin binding (Fig. 6D). KEGG analyses indicated that SSH proteins in NaHS-treated UA relate to several pivotal pathways, including vascular smooth muscle contraction (Fig. 7), focal adhesion (Supplementary Fig. S1) (31), ECM-receptor interaction (Supplementary Fig. S2) (31), regulation of actin skeleton (Supplementary Fig. S3) (31), and motor proteins (Supplementary Fig. S4) (31).

Verification of Pregnancy-dependent H_2S-reponsive Human UA SSH Proteins

KEGG analyses revealed that human UA SSH proteins were associated with various biological pathways (Fig. 7 and Supplementary Figs. S1–S4 (31)) important for vascular regulation, including vascular smooth muscle contraction (α-smooth muscle actin/ACTA1), focal adhesion (TLN1 and VCL), regulation of actin skeleton (ACTN1), VCL and CFL1, and cytoskeletal motor activity (MYH11). Direct proteomic profiling by the low-pH QTRP platform revealed that SSH-VIM was the only SSH protein detected in untreated UA sulfhydromes, whereas SSH-ACTA1, SSH-TLN1, SSH-VCL, SSH-CFL1, and SSH-ACTN1 were identified in NaHS-treated UA sulfhydromes. We further analyzed the SSH peptides/proteins in NP and P UAs that were treated with NaHS and presented the pregnancy-dependent DRSPs in a heatmap (Fig. 8A). One SSH-peptide from SSH-VIM was only detected in P UA, whereas multiple SSH peptides were identified in SSH-ACTA1, SSH-TLN1, SSH-VCL, SSH-CFL1, and SSH-ACTN1. In addition to upregulating the only SSH peptide from SSH-VIM, pregnancy also simultaneously upregulated or downregulated different SSH peptides derived from the same SSH protein (ie, SSH-ACTA1, SSH-TLN1, SSH-VCL, SSH-CFL1, and SSH-ACTN1), as listed in Supplementary Table S4 (31). Moreover, the uneven changes in the levels of different SSH peptides from the same protein make it impossible to plot SSH-proteins obtained by low-pH QTRP in heatmap for comparisons.

Finally, we determined changes of the low-pH QTRP identified SSH proteins by immunoblotting of the purified SSH proteins labeled by Tag-Switch. Baseline SSH-ACTN1, SSH-TLN1, and SSH-ACTA1 were detectable in NP UA; their levels in P UA were 1.92-fold ($P < .05$), 1.66-fold ($P < .05$), and 4.66-fold ($P < .01$), respectively, in P vs NP UAs. SSH-VIM was low in NP UA but increased by 2.70-fold ($P < .05$) in P vs NP UAs. SSH-MYH11, SSH-VCL, and SSH-CFL1 were detectable in NP UA, but their levels in P UA did not differ from that in NP UA (Fig. 8B). Total levels of ACTN1, VIM, MYH11, TLN1, ACTA1, CFL1, and VCL proteins did not differ between NP and P UA (Supplementary Fig. S5) (31).

Activation of ATP-sensitive potassium (K_{ATP}) channels mediates the vasodilatory effect of H_2S in systemic arteries via SSH of its pore-forming subunit Kir6.1 (23) and its ATP-binding cassette protein SUR2B subunit (36), which were not detected in human UA sulfhydrome by using low-pH QTRP. Immunoreactive Kir6.1 and SUR2B proteins were detectable in NP and P UA. Kir6.1 level in P UA was 1.23-fold ($P < .001$) that of NP UA, whereas SUR2B level did not differ significantly. Immunoblotting of purified SSH proteins labeled by Tag-Switch showed that baseline SSH-Kir 6.1 and SSH-SUR2B were still detectable in NP UA and that their levels in P UA were 2.69-fold ($P < .05$) and 1.71-fold ($P < .01$) that of NP UA, respectively (Fig. 8C).

Discussion

Local UA endothelium and smooth muscle H_2S production is significantly upregulated during pregnancy, which is also stimulated by endogenous and exogenous estrogens (11, 13, 14, 37, 38) and VEGF (15, 39). Augmented H_2S production contributes to human UA relaxation at least in part through activation of large conductance Ca^{2+}-activated voltage-dependent potassium (BK_{Ca}) channels (16) and stimulates endometrial and placental angiogenesis (40, 41). Vasodilation and angiogenesis are the 2 key mechanisms that promote uterine blood flow during pregnancy (42). Thus, H_2S has been emerging as a "new" UA proangiogenic vasodilator at the maternal-fetal interface, where it plays a role in uterine and placental hemodynamics regulation. However, how H_2S achieves these functions is unknown. Because sulfhydration is a major mechanism that mediates H_2S actions, we performed comprehensive proteomic analyses of sulfhydrated proteins in NP and P human UAs treated with and without an H_2S donor NaHS to uncover the targeted proteins affected by endogenous and exogenous H_2S during pregnancy. We obtained a total of 408 SSH proteins from NP and P human UAs, and this number increased to 1218 on NaHS treatment. Bioinformatics analyses of the pregnancy-dependent
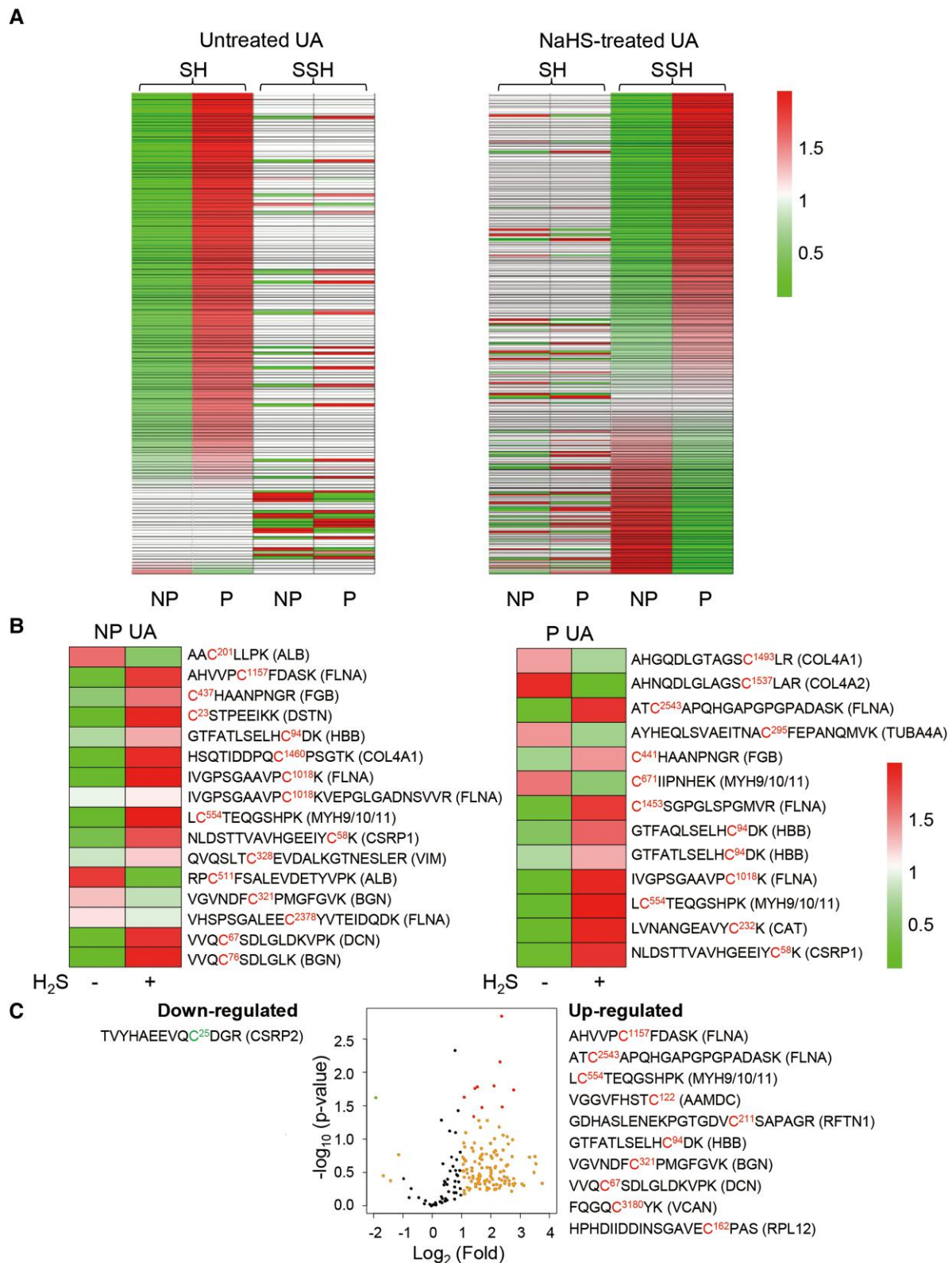
A

B

C

Figure 4. Analysis of SH and SSH peptides: effects of pregnancy and NaHS. (A) Heatmap of SH-peptides and SSH-peptides from untreated (left panel) and NaHS-treated (right panel) nonpregnant (NP) and pregnant (P) human uterine arteries (UA). The intensity values of unidentified SH-peptides and SSH-peptides in conditions were assigned with 1. (B) Heatmap showing H_2S-responsive SSH-peptides in NP (left panel) and P (right panel) human UAs. SSH-peptides that were repeatedly present ($n > 2$) were counted. (C) Volcano plot showing differentially regulated SSH-peptides in NaHS-treated NP and P human UA. The SSH-peptide with a $P < 0.05$ and a |$\log_2$Fold Change| > 1 was considered as significantly differentially regulated. SSH-peptides that were repeatedly present ($n > 2$) were counted. Upregulated peptides (fold change > 2) and downregulated peptides (fold change < 0.5) were shown in the plot.
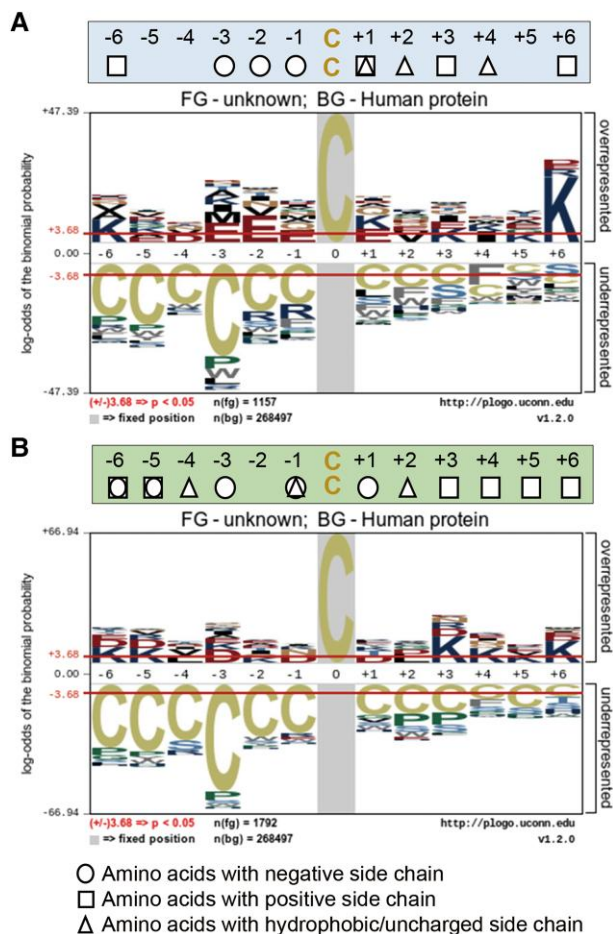
Figure 5. Modeling of consensus motifs of putative SSH peptide. Comparison of calculated sequence motifs of (A) SSH- (1157 sequences as inputs) and (B) SH-cysteines (1792 sequences as inputs). Images were generated with pLogo and scaled to the height of the largest column within the sequence visualization. The red horizontal lines on the pLogo plots denote $P = 0.05$ thresholds.

H$_2$S-responsive human UA sulfhydrome demonstrate that these sulfhydrated proteins are linked to a plethora of biological processes and pathways as well as molecular functions, informing novel roles of protein sulfhydration in uterine hemodynamics regulation.

Sulfhydration was initially described in 2009 as a posttranslational modification (PTM) on cysteine on proteins with importance comparable to that of S-nitrosylation (SNO) and phosphorylation (17), but it has been gained momentum in research lately because of recent discoveries of its role in diverse biological processes in physiology and pathophysiology. SSH converts -SH group at cysteines to -SSH groups, typically occurring on reactive cysteine(s) with a low pK_a. However, the intrinsically unstable nature of the S-SH bond makes it challenging to detect its changes in complex biological samples. A modified biotin Tag-Switch assay was initially developed to detect SSH, in which unmodified cysteines are blocked by methyl methanethiosulfonate, whereas SSH-cysteines is reduced by DTT to -SH that is then labeled with biotin to be readily captured with avidin and quantified by immunoblotting (17). Other indirect methods are then developed to improve specificity, involving selectively labeling SSH such as the Tag-Switch method that uses MSBT-A to block SH groups, whereas a reagent incorporating a nucleophilic

component and a biotin reporter moiety selectively labels SSH groups (27). In addition, a quantitative persulfide site identification (QPers-SID) method based on selective elution of persulfides using a reducing agent has also been developed for indirect site-directed identification of SSH proteins via LC-MS/MS (43). More recently, a low-pH QTRP proteomics platform has made it possible to directly analyze protein sulfhydration at a proteome scale in cells in vitro (30) and multicell organisms such as *Caenorhabditis elegans* in vivo (44). These studies signify significant advancements in SSH detection methods and redox biology.

Quantification of total SSH proteins by using Tag-Switch labeling and immunoblotting has shown that pregnancy increases protein sulfhydration human UA. In these assays, addition of a reducing agent DTT significantly reduces total levels of SSH proteins, indicating that SSH proteins are sensitive to reducing conditions. Treatment with exogenous H$_2$S increases total levels of SSH proteins in NP UA to that in untreated P UA but does not significantly alter total levels of SSH proteins in P UA. These results suggest that protein sulfhydration in human UA may be maximized by augmented endogenous H$_2$S during pregnancy in vivo. However, mapping site-specific human UA sulfhydrome by low-pH QTRP has shown great shifts in SH peptides/SH proteins to SSH peptides/SSH proteins in NP vs P UAs by exogenous H$_2$S, suggesting that endogenous and exogenous H$_2$S differentially regulate protein sulfhydration.

Here, low-pH QTRP platform is used to further map site-specific SSH proteins directly in human UA tissues treated with NaHS. We have identified a total of 1617 SSH peptides from 1218 SSH-proteins in the human UA sulfhydrome. The total SSH sites and SSH proteins in human UA sulfhydrome are less than these in the human endothelial cell Sulfhydrome, as reported in a recent study (45). In that study, QPers-SID was used to map human endothelial cell sulfhydrome, which contains a total of 3446 individual SSH sites from 1591 SSH proteins in shear stress-treated human endothelial cells in vitro. Human UA sulfhydrome overlaps 110 SSH proteins in human endothelial cell sulfhydrome mapped by QPers-SID, including proteins of muscle structural and cytoskeleton functions (ie, MYH9/10, VIM, FLNA, and ACTN1) and redox signaling (ie, glyceraldehyde 3-phosphate dehydrogenase and mitochondrial dihydrolipoyl dehydrogenase, and thioredoxins) (46). However, the number of SSH peptides/proteins in untreated human UA tissues is much greater than that reported in human serum previously (30), showing that low-pH QTRP platform is capable of direct mapping site-specific sulfhydrome in biospecimens under physiological conditions.

Endogenous H$_2$S is a pluripotent gaseous signal that regulates various reproductive processes. In males, H$_2$S protects spermatogenic failure and testicular dysfunction because of its potent anti-inflammatory and antioxidative effects (47). In females, granulosa cells derived endogenous H$_2$S regulates ovulation potentially by promoting follicle rupture (48). CBS-derived H$_2$S regulates oviduct transportation of embryos (49) and decidualization (50). CBS/CSE-derived H$_2$S maintains uterine quiescence via suppressing inflammation and the expression of myometrial contractile proteins in human pregnancy (51). Human trophoblast–derived H$_2$S regulates placental angiogenesis (40) and plays a role in maternal–fetal immune hemostasis during early pregnancy (52). Endometrial stroma–derived H$_2$S regulates microvascular endothelial cell angiogenesis in the menstrual cycle and pregnancy in women (41). Dysregulated H$_2$S signaling results in preeclampsia-like
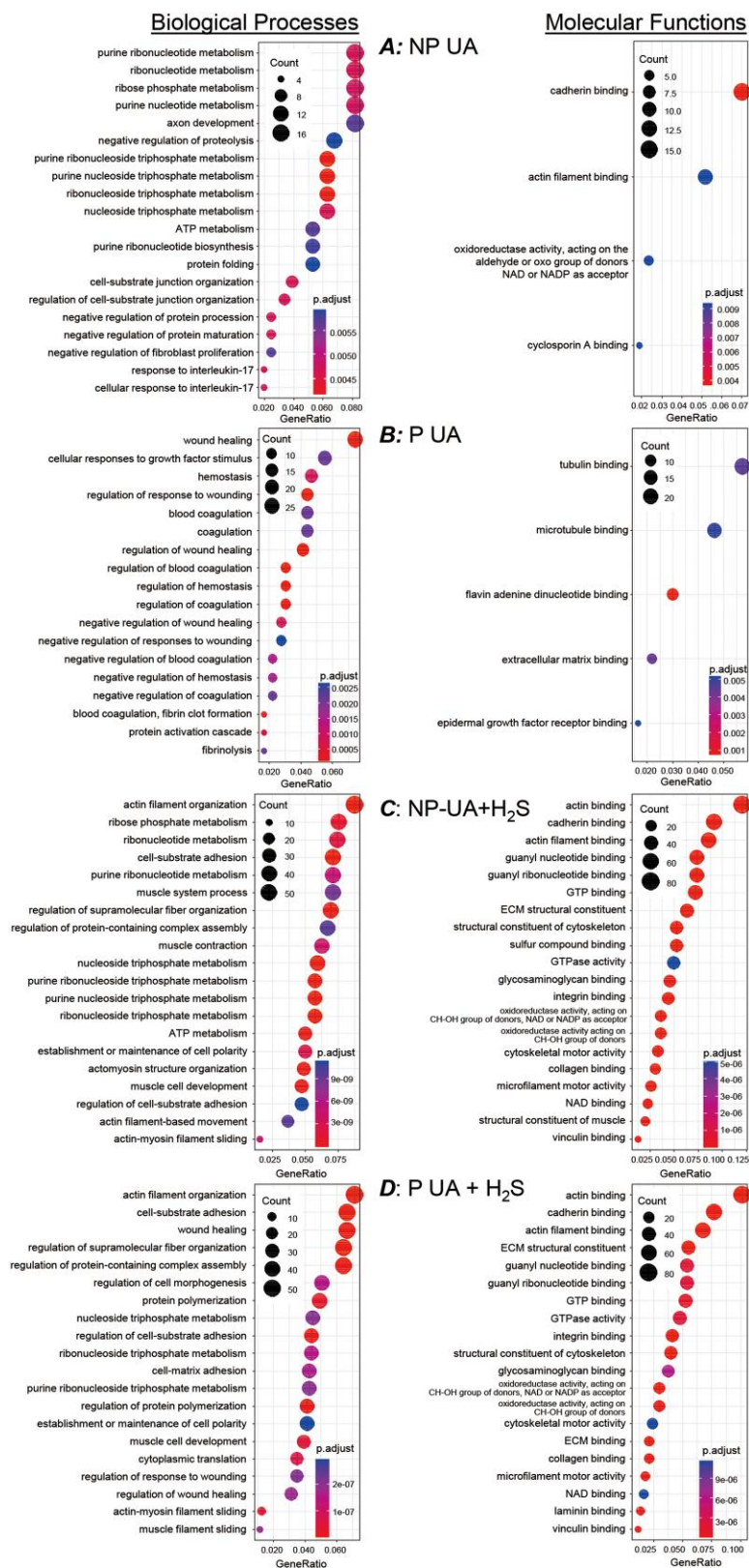
Figure 6. Functional analysis of pregnancy-dependent H_2S-reponsive human UA SSH proteins. Significantly ($P < 0.01$) enriched gene ontology (GO) terms of biological processes and molecular functions among differentially regulated SSH proteins (DRSPs) are visualized in left and right panels, respectively. Each dot is proportional in size to the number of SSH-proteins associated with the term. The DRSPs were unique in NP (A) and P (B) untreated UA, and NP (C) and P (D) UA treated with NaHS.
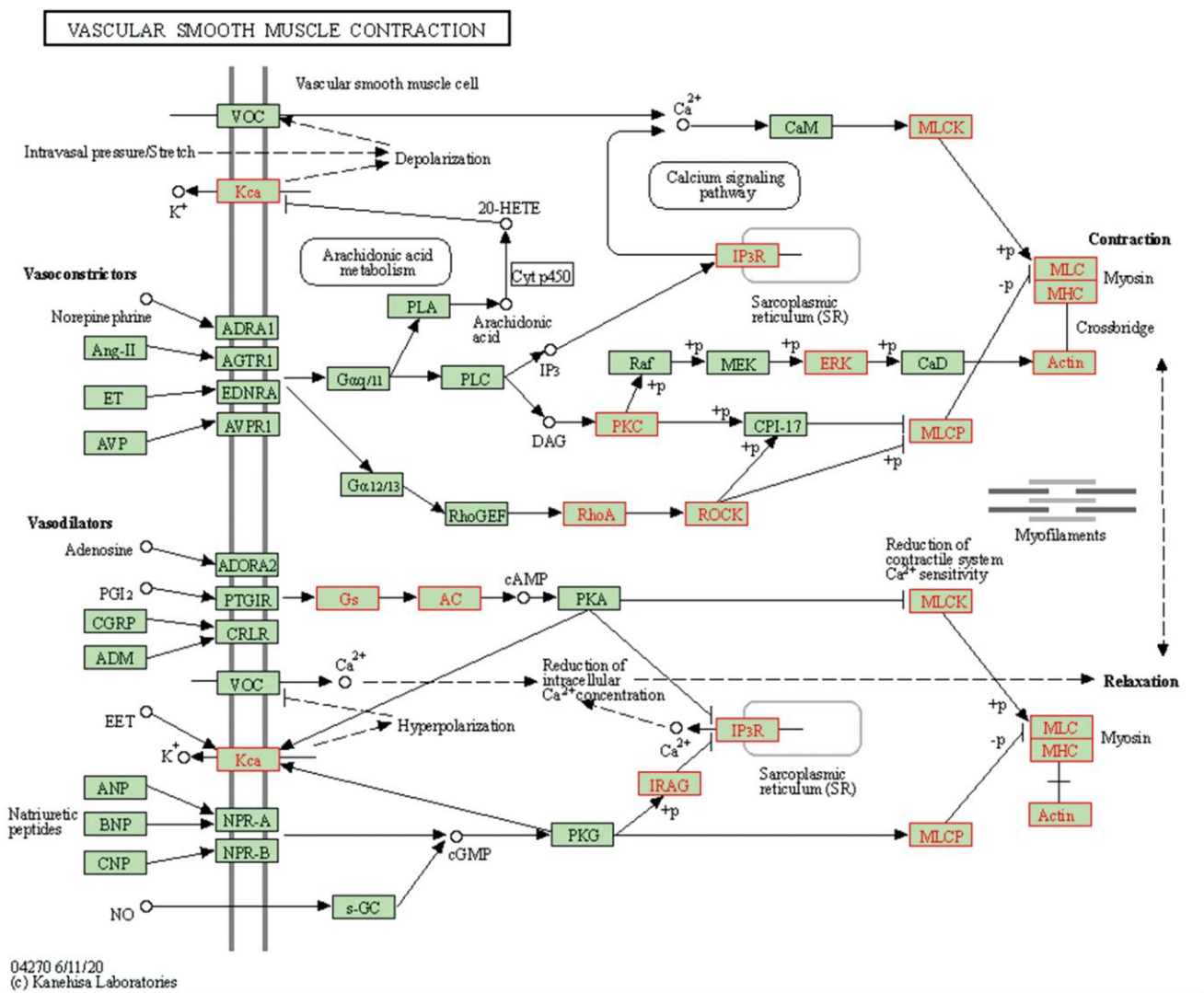
Figure 7. KEGG pathway analysis revealed that sulfhydrated proteins regulate vascular smooth muscle contraction. The identified SSH proteins in pregnancy-dependent H_2S-responsive human uterine artery sulfhydrome were subjected to KEGG pathway analysis to map the network. The network initiates from extracellular stimuli such as intravasal pressure/stretch, vasoconstrictors (angiotensin II/Ang2, endothelin, vasopressin/AVP, vasodilators [prostacyclin/PGI2, calcitonin gene-related peptides/CGRPs, adrenomedullin/ADM, epoxyeicosatrienoic acids/EETs, natriuretic peptides/NPs]), acting through corresponding membrane receptors and/or channels to (de)polarize plasma membrane, activating effectors (G-proteins) and various cytosolic signaling pathways (Ca^{2+} signaling, arachidonic acid metabolism, phospholipases [PLA/PLC], protein kinases [PKA, PKC, and PKG]); these signaling pathways collectively activate myosin light-chain kinase (MLCK) to (de)phosphorylate myosins that harmonize muscle contraction and relaxation. Significantly ($P < 0.01$) enriched Kyoto Encyclopedia of Genes and Genomes (KEGG) terms among SSH proteins were mapped in the KEGG pathways as archived in the KEGG module database (https://www.genome.jp/kegg/module.html).

syndromes because of impaired angiogenesis, trophoblast invasion, and impaired uterine spiral artery remodeling, leading to adverse fetal outcomes including intrauterine growth restriction, placental abruption, and fetal demise in utero (24). Although the clinical importance of H_2S signaling has been appreciated in diverse reproductive processes, especially in pregnancy, further revealing the specific pathways and biological processes activated by H_2S in these processes is required to underscore future therapeutic potentials.

Our bioinformatics analyses have shown that among the many biological processes, pathways, and molecular functions that are linked to the SSH proteins in the human UA sulfhydrome, pregnancy-dependent H_2S-responsive DRSPs are mostly vascular smooth muscle proteins (FLNA and MYH11) and ECM proteins (raftlin 1, BGN, DCN, and versican core protein), with different responses to endogenous

and exogenous H_2S. DRSPs between NP and P UAs, presumptively from endogenous H_2S that is augmented in pregnancy, are proteins forming microtubules and ECM, implicating that sulfhydration is involved in vascular wall remodeling during uterine artery adaptation to pregnancy (53). Interestingly, we found the biological processes of nucleotide metabolisms and wound healing are exclusively shown in NP and P unique DRSPs, respectively, suggesting that transcriptional activity is highly active in NP UA, whereas angiogenic capillaries can invade wound clots and quickly form microvascular networks in the P state. The DRSPs in response to exogenous H_2S are proteins linked to pathways of vascular smooth muscle contraction, ECM, and redox biology, which are present in both NP and P UAs. For instance, ACTA1 and TLN1 are H_2S-responsive DRSPs that are directly linked to mechanical coupling actin cytoskeleton with integrins (54, 55).

A

NP	fold	P	SSH-peptide (Protein)
	1.34		QVQSLTC^{328}EVDALKGTNESLER (VIM)
	1.14		VGELC^{343}AGK (VCL)
	0.78		EILGTC^{325}K (VCL)
	7.22		REILGTC^{326}K (VCL)
	0.97		C^{545}DRVDQLTAQLADLAAR (VCL)
	3.68		VENAC^{88}TK (VCL)
	1.28		ALIQC^{1018}AK (VCL)
	2.59		TNLLQVC^{1053}ER (VCL)
	8.97E+06		IAELC^{422}DDPKER (VCL)
	3.72E+06		KIAELC^{422}DDPKER (VCL)
	0.23		MLPDKDC^{80}R (CFL1)
	4.56		HELQANC^{139}YEEVK (CFL1)
	5.25		HELQANC^{139}YEEVKDR (CFL1)
	4.23		C^{147}TLAEK (CFL1)
	2.79		NC^{286}GQMSEIEAK (TLN1)
	1.00		VVAPTISSPVC^{732}QEQLVEAGR (TLN1)
	0.60		ASAGPQPLLVQSC^{956}K (TLN1)
	0.58		ASVPTIQDQASAMQLSQC^{1023}AK (TLN1)
	1.88		VQELGHGC^{1927}AALVTK (TLN1)
	0.63		AGALQC^{1939}SPSDAYTK (TLN1)
	0.61		AGALQC^{1939}SPSDAYTKK (TLN1)
	0.54		ELIC^{1953}AR (TLN1)
	1.14E+07		KELIC^{1953}AR (TLN1)
	0.80		MVAAATNNLC^{2408}EAANAAVQGHASQEK (TLN1)
	1.58E-05		QELAVFC^{2161}SPEPPAK (TLN1)
	1.06		C^{2196}TQDLGNSTK (TLN1)
	6.27E+05		QVAASTAQLLVAC^{2442}K (TLN1)
	2.21		VEDMAELTC^{91}LNEASVLHNLR (MYH11)
	0.17		EDQSILC^{172}TGESGAGK (MYH11)
	1.00		EDQSILC^{172}TGESGAGKTENTK (MYH11)
	0.70		SMLQDREDQSILC^{176}TGESGAGK (MYH11)
	0.59		SMLQDREDQSILC^{176}TGESGAGKTENTK (MYH11)
	2.73E-06		VC^{362}HLMGINVTDFTR (MYH11)
	1.55		LC^{554}TEQGSHPK (MYH11)
	4.18		C^{671}IIPNHEK (MYH11)
	5.97E+06		QAC^{747}ILMIK (MYH11)
	2.85		NC^{923}AAYLK (MYH11)
	1.48		EGLLLWC^{154}QR (ACTN1)
	1.21		C^{332}QLEINFNTLQTK (ACTN1)
	0.86		MVSDINNAWGC^{370}LEQVEK (ACTN1)
	1.00		RELPPDQAEYC^{860}IAR (ACTN1)
	2.55E+06		LC^{219}YVALDFENEMATAASSSSLEK (ACTA1)
	1.18		EKLC^{219}YVALDFENEMATAASSSSLEK (ACTA1)
	0.45		C^{259}PETLFQPSFIGMESAGIHETTYNSIMK (ACTA1)
	1.21E-05		FRC^{259}PETLFQPSFIGMESAGIHETTYNSIMK (ACTA1)
	0.73		C^{287}DIDIR (ACTA1)
	0.37		C^{287}DIDIRK (ACTA1)
	2.10E-05		C^{287}DIDIRKDLYANNVLSGGTTMYPGIADR (ACTA1)

Legend scale: 1.5 — 1 — 0.5

B

NP   P

SSH-ACTN1
ACTN1
SSH-VIM
VIM
SSH-MYH11
MYH11
SSH-TLN1
TLN1
SSH-ACTA1
ACTA1
SSH-CFL1
CFL1
SSH-VCL
VCL

Bar graph (SSH-Protein, fold; 0–5): ACTN1 *, VIM *, MYH11 ns, TLN1 *, ACTA1 **, CFL1 ns, VCL ns. Legend: P, NP.

C

SSH-Kir 6.1
Kir 6.1
SSH-SUR2B
SUR2B
β-actin

Bar graphs: Protein (fold): SUR2B ***, Kir 6.1. SSH-Protein (fold): SUR2B *, Kir 6.1 **.
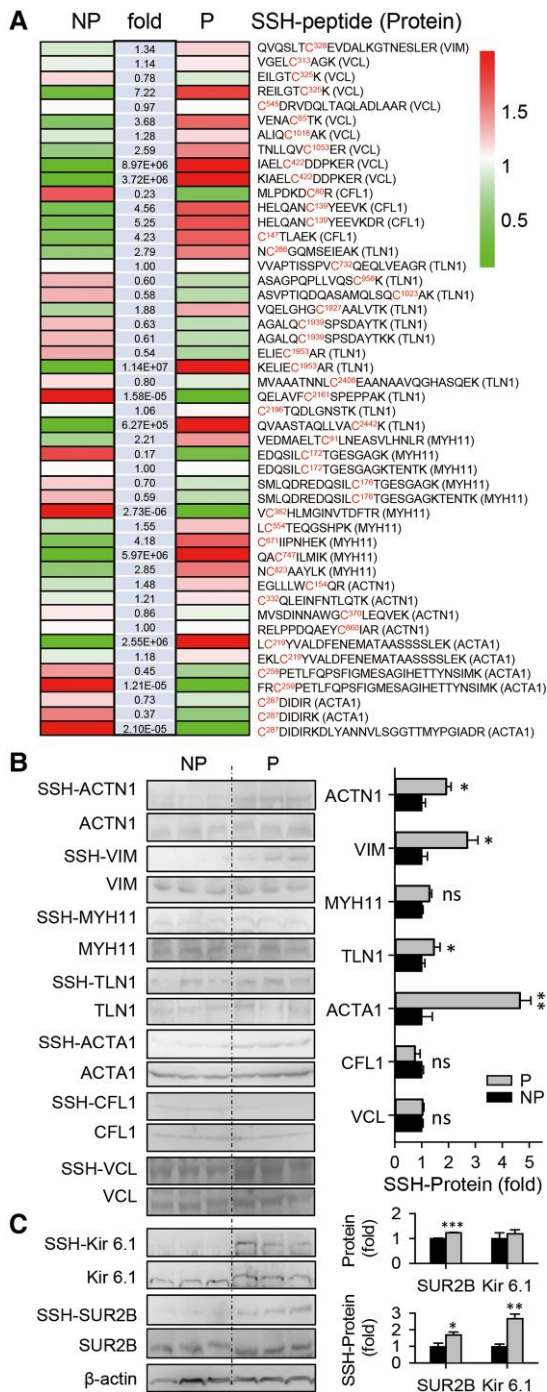
Figure 8. Identification of vascular smooth muscle contraction/relaxation related SSH proteins in human uterine artery. (A) The intensity values of SSH peptides from the typical muscle contraction-related proteins identified by low-pH QTRP from NaHS-treated nonpregnant (NP) and pregnant (P) human uterine arteries (UAs) were used to generate the heatmap of pregnancy-dependent changes. The intensity values of the SSH peptides were assigned with 1 when unidentified in 1 condition; the fold changes were differences of their intensities between P and NP UAs (n = 3/group). The SSH peptides listed were vascular smooth muscle contraction-related proteins including from VIM, VCL, CFL1, TLN1, MYH11, ACTN1, and ACTA1. Immunoblotting of Tag-Switch–labeled total SSH proteins in NP and P human UA to verify SSH proteins identified (B) and to detect K_{ATP} channels unidentified (C) by low-pH QTRP. Bar graphs summarized pregnancy-dependent changes in SSH proteins (B) and total/SSH proteins of K_{ATP} channels. Data (mean ± standard error of the mean) were presented as fold of controls. *$P < 0.05$, **$P < 0.01$, ***$P < 0.001$ vs control.

Another human UA H_2S-responsive DRSP is integrin β1. Interestingly, integrins are the most abundant SSH proteins in the human endothelial cell sulfhydrome, and SSH of integrin β3 is required for endothelial cell mechanotransduction in vitro and flow-induced dilation in mouse mesenteric arteries in vivo (45). Thus, SSH of integrin β1 may play a role in endothelium-dependent mechanisms of the uterine vasodilatory effects of H_2S. Other pregnancy-dependent DRSPs in human UA sulfhydrome are peroxiredoxins 1 through 4 and superoxide dismutase; these proteins are responsive to exogenous H_2S as shown in previous studies, which regulate cell redox homeostasis (30). Phosphodiesterase type 5 (PDE5A) is another pregnancy-dependent DRSP in human UA, and is also responsive to exogenous H_2S. PDE5 is a key enzyme that breaks down the second messenger cyclic GMP (cGMP) that mediates NO-mediated vasodilation. Previous studies have shown that H_2S enhances PDE5A sulfhydration to inhibit its dimerization, thereby inhibiting cGMP degradation and activating the cGMP/PKG pathway for vascular relaxation (56, 57). However, the specific SSH cysteine has not been identified. Our current study has first identified Cys149 (FDHDEGDQC149SR) as the only SSH site in PDE5A, suggesting that SSH of PDE5A at Cys149 plays a physiological role in mediating H_2S interactions with NO in uterine hemodynamics regulation.

Since SSH is a PTM occurring at 1 or more specific reactive cysteine(s), quantitatively measurement of changes in SSH at each specific cysteine is needed for functional analysis of a given SSH protein. The low-pH QTRP platform provides a powerful tool for direct mapping site-specific protein sulfhydration with measurement of changes of all SSH sites in all SSH proteins in paired proteomes simultaneously (29). In human UA sulfhydrome, we have observed 3 patterns of SSH on specific cysteines in different proteins. First, SSH occurs in a protein at only 1 cysteine in some structural proteins such as VIM at Cys328 with higher level in P vs NP UA. Interestingly, Cys328 SSH-VIM is also greater in endothelial cells (with greater endogenous H_2S) isolated from plaque-free than plaque-containing mesenteric arteries (45), suggesting that SSH of VIM at Cys328 is involved in physiological and pathophysiological processes in association with endogenous H_2S. Second, SSH occurs in a protein at multiple cysteines and levels of the multiple SSH peptides from the same protein change in the same direction such as lactate dehydrogenase A (LDHA). SSH of LDHA occurs at Cys131 and Cys163 and the 2 SSH peptides containing Cys131 and Cys163 are greater in P vs NP UA. Exogenous H_2S dose-dependently increases SSH-LDHA in HCT116 cells and a C163A mutation decreases LDHA catalytic activity in response to H_2S stimulation (57). Third, SSH occurs in a protein at multiple cysteines and levels of the SSH peptides from the same protein change in opposite directions such as cofilin 1 (CFL1) with 3 SSH-peptides containing Cys80, Cys139, and Cys147; levels of the SSH peptide containing Cys80 is greater in NP vs P UA, whereas SSH peptides containing Cys139 and Cys147 are greater in P vs P UA. The opposite patterns of changes in levels of these SSH peptides may be the reason that total levels of SSH-CFL1 does not differ in P vs NP UA when quantified by immunoblotting of total SSH proteins labeled by Tag-Switch (Fig. 8). This also makes it impossible to visualize changes of SSH proteins in heatmap, similar to proteomics data analyses of other PTMs (44). We previously reported that SNO occurs in CFL1 at 4 cysteines (39/80/139/147),

but only SNO at Cys80/139 mediates endothelial cytoskeleton remodeling and migration on VEGF and estradiol stimulation (58, 59). In general, SNO and SSH regulate protein function paradoxically (17). Thus, our studies show that SSH and SNO may occur at the same or different cysteines in a protein to mediate NO and H_2S interactions in uterine hemodynamics regulation and potentially in any other physiological regulations.

Unique consensus motifs facilitate sulfhydration at thiol groups in specific cysteines. By modeling the flanking sequences of cysteine-containing SSH peptides and SH peptides in our human UA sulfhydrome and datasets in other studies (22, 30, 34), we have obtained the intrinsic characteristics of consensus amino acid sequence containing a cysteine to be putatively sulfhydrated. A putative consensus sequence of SSH site contains negatively charged acidic amino acid Glu (E) at positions -1, -2, -3, and $+1$ to SSH-cysteine. Except acidic amino acid Asp (D) at positions -1 and $+1$, negatively charged amino acids are less frequently present in proximity to SH-cysteine. The protonated Glu is capable of lowering pKa of an adjacent thiol by forming a hydrogen bond, the presence of overrepresented Glu in close proximity to a cysteine can result in reduced pKa, possibly promoting deprotonation and SSH formation. A unique observation is that cysteine is underrepresented near the SSH-cysteine(s), offering an explanation why SSH only occurs at unique but not all cysteine(s). Nonetheless, our modeling analyses show that SSH occurs at specific cysteine(s) surrounded by acidic amino acids without other cysteine(s) in proximity.

The total numbers of SSH peptides and SSH proteins in human UA identified by low-pH QTRP platform increase significantly after the samples are treated with exogenous H_2S, suggesting potential limitations of the method in direct proteomic profiling protein sulfhydration in tissue samples associated with endogenous H_2S. VCL and ACTN1 bind to actin filaments to form the actin bundles, playing a regulatory role in actin cytoskeleton as shown in our KEGG analysis (Supplementary Fig. S4) (31). However, SSH-VCL along with others (SSH-ACTA1, SSH-MYH11, SSH-TLN1, and SSH-ACTN1) important for cytoskeleton remodeling and muscle function are only detected in NaHS-treated human UA by low-pH QTRP. However, when total SSH proteins from untreated NP and P human UA samples are enriched by Tag-Switch labeling followed by avidin purification, we show pregnancy-dependent changes in SSH in these proteins (Fig. 8B), suggesting a crucial role of protein sulfhydration in smooth muscle contraction/relaxation that underlines the major mechanism for vascular tone regulation.

Of specific interest, we hoped to identify the specific K^+ channels to be sulfhydrated in human UA because K_{ATP} and BK_{Ca} channels are known to be important for uterine hemodynamics regulation in pregnancy (60-64). BK_{Ca} channels at least partially mediates H_2S stimulation of human UA relaxation in vitro (16). Interestingly, low-pH QTRP identified the BK_{Ca} channel pore-forming α-subunit (KCNMA1/BKα) as a target of SSH, which is only identified in pregnant human UA as listed in Supplementary Table S3 (31). Particularly, Cys710 (MRRAC710CFDCGR) is the specific SSH site in BKα. This suggests a role of SSH in BK_{Ca} channel activation in pregnancy-associated uterine vasodilation, although how SSH-BKα activates BK_{Ca} channels needs to be further delineated. Activation of vascular smooth muscle K_{ATP} channels is the first mechanism known to mediate the vasodilatory

effects of H_2S in systemic arteries (20, 65), which is achieved through SSH of Kir6.1 at Cys43 (23) and SUR2B at Cys24 and Cys2455 (36). Unexpectedly, low-pH QTRP fails to dig out these proteins in human UA even after treated with exogenous H_2S. However, herein we show that immunoblotting with specific antibodies can detect SSH-Kir6.1 and SSH-SUR2B in enriched total human UA SSH proteins and that levels of SUR2B and SSH-Kir6.1 and SSH-SUR2B are significant greater in P versus NP human UA, suggesting a role of K_{ATP} channels and their sulfhydration in pregnancy-associated UA dilation; although how pregnancy affects SSH of K_{ATP} channels in human UA is currently elusive, this seems not to be directly related to enhanced H_2S production because K_{ATP} channels seem not to play a key in H_2S-stimulated human UA relaxation in vitro (16). Nonetheless, this shows another limitation of low-pH QTRP in identification of SSH in low expression/abundance proteins. Although identification of SSH of low-abundance proteins of importance can be achieved by immunoblotting of enriched samples using Tag-Switch labeling followed by avidin purification, peptide sequencing is still needed to identify specific SSH site(s) for functional analysis.

In summary, our current study provides the initial datasets about the targeted proteins in human UA associated with augmented endogenous H_2S in pregnancy and influenced by exogenous H_2S to inform novel diverse roles of protein sulfhydration in uterine hemodynamics regulation. In keeping with the emerging roles of H_2S in uterine hemodynamics regulation, additional functional studies are needed to further elucidate the importance of sulfhydration in specific pathway(s) that H_2S activates to mediate its uterine proangiogenic and vasodilatory effects in pregnancy and pregnancy complications.

Acknowledgments

Funding

Disclosures

All authors declare no financial interests. D.B.C. is a current member of the Editorial Board of *Endocrinology*, but with no access to the handling and peer review of this study.

Data Availability

Original data presented in the study are included in the article and Supplementary Data (https://dataverse.harvard.edu/dataset.xhtml?persistentId=doi%3A10.7910%2FDVN%2FRQMEBW&version=DRAFT). Further inquiries can be directed to the corresponding author.

References

1. Rosenfeld CR. Distribution of cardiac output in ovine pregnancy. *Am J Physiol*. 1977;232(3):H231-H235.
2. Palmer SK, Zamudio S, Coffin C, Parker S, Stamm E, Moore LG. Quantitative estimation of human uterine artery blood flow and pelvic blood flow redistribution in pregnancy. *Obstet Gynecol*. 1992;80(6):1000-1006.
3. Redman CW, Sargent IL. Latest advances in understanding preeclampsia. *Science*. 2005;308(5728):1592-1594.
4. Ives Christopher W, Sinkey R, Rajapreyar I, Tita Alan TN, Oparil S. Preeclampsia—pathophysiology and clinical presentations. *J Am Coll Cardiol*. 2020;76(14):1690-1702.
5. Gluckman PD, Hanson MA, Cooper C, Thornburg KL. Effect of in utero and early-life conditions on adult health and disease. *N Engl J Med*. 2008;359(1):61-73.
6. Osol G, Ko NL, Mandala M. Altered endothelial nitric oxide signaling as a paradigm for maternal vascular maladaptation in preeclampsia. *Curr Hypertens Rep*. 2017;19(10):82.
7. Trapani A Jr, Goncalves LF, Trapani TF, Vieira S, Pires M, Pires MMS. Perinatal and hemodynamic evaluation of sildenafil citrate for preeclampsia treatment: a randomized controlled trial. *Obstet Gynecol*. 2016;128(2):253-259.
8. Sharp A, Cornforth C, Jackson R, *et al*. Maternal sildenafil for severe fetal growth restriction (STRIDER): a multicentre, randomised, placebo-controlled, double-blind trial. *Lancet Child Adolesc Health*. 2018;2(2):93-102.
9. Wang R. Physiological implications of hydrogen sulfide: a whiff exploration that blossomed. *Physiol Rev*. 2012;92(2):791-896.
10. Filipovic MR, Zivanovic J, Alvarez B, Banerjee R. Chemical biology of H$_2$S signaling through persulfidation. *Chem Rev*. 2018;118(3):1253-1337.
11. Lechuga TJ, Zhang H-H, Sheibani L, *et al*. Estrogen replacement therapy in ovariectomized nonpregnant ewes stimulates uterine artery hydrogen sulfide biosynthesis by selectively up-regulating cystathionine beta-synthase expression. *Endocrinology*. 2015;156(6):2288-2298.
12. Lechuga TJ, Qi Q-R, Magness RR, Chen D-B. Ovine uterine artery hydrogen sulfide biosynthesis in vivo: effects of ovarian cycle and pregnancy. *Biol Reprod*. 2019;100(6):1630-1636.
13. Sheibani L, Lechuga TJ, Zhang HH, *et al*. Augmented H$_2$S production via CBS upregulation plays a role in pregnancy-associated uterine vasodilation. *Biol Reprod*. 2017;96(3):664-672.
14. Bai J, Lechuga TJ, Makhoul J, *et al*. ERα/ERβ-directed *CBS* transcription mediates E2β-stimulated huaec H$_2$S production. *J Mol Endocrinol*. 2023;70(2):e220175.
15. Bai J, Chen D-B. Enhanced Sp1/YY1 expression directs *CBS* transcription to mediate VEGF-stimulated pregnancy-dependent H$_2$S production in human uterine artery endothelial cells. *Hypertension*. 2021;78(6):1902-1913.
16. Li Y, Bai J, Yang YH, Hoshi N, Chen DB. Hydrogen sulfide relaxes human uterine artery via activating smooth muscle BKCa channels. *Antioxidants (Basel)*. 2020;9(11):1127.
17. Mustafa AK, Gadalla MM, Sen N, *et al*. H$_2$S signals through protein S-sulfhydration. *Sci Signal*. 2009;2(96):ra72.
18. Sen N, Paul DB, Gadalla MM, *et al*. Hydrogen sulfide-linked sulfhydration of NF-kB mediates its antiapoptotic actions. *Mol Cell*. 2012;45(1):13-24.
19. Mustafa AK, Gadalla MM, Snyder SH. Signaling by gasotransmitters. *Sci Signal*. 2009;2(68):re2.
20. Zhao W, Zhang J, Lu Y, Wang R. The vasorelaxant effect of H$_2$S as a novel endogenous gaseous K$_{ATP}$ channel opener. *EMBO J*. 2001;20(21):6008-6016.
21. Kondo K, Bhushan S, King AL, *et al*. H$_2$S protects against pressure overload-induced heart failure via upregulation of endothelial nitric oxide synthase. *Circulation*. 2013;127(10):1116-1127.
22. Gao X-H, Krokowski D, Guan B-J, *et al*. Quantitative H$_2$S-mediated protein sulfhydration reveals metabolic reprogramming during the integrated stress response. *Elife*. 2015;4:e10067.
23. Mustafa AK, Sikka G, Gazi SK, *et al*. Hydrogen sulfide as endothelium-derived hyperpolarizing factor sulfhydrates potassium channels. *Circ Res*. 2011;109(11):1259-1268.
24. Wang K, Ahmad S, Cai M, *et al*. Dysregulation of hydrogen sulfide producing enzyme cystathionine γ-lyase contributes to maternal hypertension and placental abnormalities in preeclampsia. *Circulation*. 2013;127(25):2514-2522.
25. Szabo C, Coletta C, Chao C, *et al*. Tumor-derived hydrogen sulfide, produced by cystathionine-β-synthase, stimulates bioenergetics, cell proliferation, and angiogenesis in colon cancer. *Proc Natl Acad Sci U S A*. 2013;110(30):12474-12479.
26. Zivanovic J, Kouroussis E, Kohl JB, *et al*. Selective persulfide detection reveals evolutionarily conserved antiaging effects of S-sulfhydration. *Cell Metab*. 2019;30(6):1152-1170.e13.
27. Zhang D, Macinkovic I, Devarie-Baez NO, *et al*. Detection of protein S-sulfhydration by a tag-switch technique. *Angew Chem Int Ed Engl*. 2014;53(2):575-581.
28. Aroca A, Benito JM, Gotor C, Romero LC. Persulfidation proteome reveals the regulation of protein function by hydrogen sulfide in diverse biological processes in arabidopsis. *J Exp Bot*. 2017;68(17):4915-4927.
29. Fu L, Li Z, Liu K, *et al*. A quantitative thiol reactivity profiling platform to analyze redox and electrophile reactive cysteine proteomes. *Nat Protoc*. 2020;15(9):2891-2919.
30. Fu L, Liu K, He J, Tian C, Yu X, Yang J. Direct proteomic mapping of cysteine persulfidation. *Antioxid Redox Signal*. 2020;33(15):1061-1076.
31. Bai J, Jiao FL, Salmeron AG, *et al*. Supplemental data to the paper: Mapping pregnancy-dependent sulfhydrome unfolds diverse functions of protein sulfhydration in human uterine artery. Harvard Dataverse. 2023. https://dataverse.harvard.edu/dataset.xhtml?persistentId=doi%3A10.7910%2FDVN%2FRQMEBW&version=DRAFT
32. Yu G, Wang L-G, Han Y, He Q-Y. Clusterprofiler: an R package for comparing biological themes among gene clusters. *OMICS*. 2012;16(5):284-287.
33. Kolde R, Kolde MR. Package 'pheatmap'. R Package. 2018;1.
34. Wu Q, Zhao B, Weng Y, *et al*. Site-specific quantification of persulfidome by combining an isotope-coded affinity tag with strong cation-exchange-based fractionation. *Anal Chem*. 2019;91(23):14860-14864.
35. O'Shea JP, Chou MF, *et al*. Plogo: a probabilistic approach to visualizing sequence motifs. *Nat Methods*. 2013;10(12):1211-1212.
36. Kang M, Hashimoto A, Gade A, Akbarali HI. Interaction between hydrogen sulfide-induced sulfhydration and tyrosine nitration in the K$_{ATP}$ channel complex. *Am J Physiol Gastrointest Liver Physiol*. 2015;308(6):G532-G539.
37. Lechuga TJ, Bilg AK, Patel BA, Nguyen NA, Qi Q-R, Chen D-B. Estradiol-17β stimulates H$_2$S biosynthesis by ER-dependent *CBS* and *CSE* transcription in uterine artery smooth muscle cells in vitro. *J Cell Physiol*. 2019;234(6):9264-9273.
38. Lechuga TJ, Qi Q-R, Kim T, Magness RR, Chen D-B. E2β stimulates ovine uterine artery endothelial cell H$_2$S production in vitro by estrogen receptor-dependent upregulation of cystathionine beta-synthase and cystathionine gamma-lyase expression. *Biol Reprod*. 2019;100(2):514-522.
39. Zhang H-H, Chen JC, Sheibani L, Lechuga TJ, Chen D-B. Pregnancy augments VEGF-stimulated in vitro angiogenesis and vasodilator (NO and H$_2$S) production in human uterine artery endothelial cells. *J Clin Endocrinol Metab*. 2017;102(7):2382-2393.

40. Chen D-B, Feng L, Hodges JK, Lechuga TJ, Zhang H. Human trophoblast-derived hydrogen sulfide stimulates placental artery endothelial cell angiogenesis. *Biol Reprod*. 2017;97(3):478-489.

41. Qi Q-R, Lechuga TJ, Patel B, *et al*. Enhanced stromal cell CBS-H$_2$S production promotes estrogen-stimulated human endometrial angiogenesis. *Endocrinology*. 2020;161(11):bqaa176.

42. Bai J, Qi QR, Li Y, Makoul J, Magness RR, Chen DB. Estrogen receptors and estrogen-induced uterine vasodilation in pregnancy. *Int J Mol Sci*. 2020;21(12):4349-4398.

43. Longen S, Richter F, Kohler Y, Wittig I, Beck KF, Pfeilschifter J. Quantitative persulfide site identification (QPers-SID) reveals protein targets of H$_2$S releasing donors in mammalian cells. *Sci Rep*. 2016;6(1):29808.

44. Meng J, Fu L, Liu K, *et al*. Global profiling of distinct cysteine redox forms reveals wide-ranging redox regulation in *c. elegans*. *Nat Commun*. 2021;12(1):1415.

45. Bibli SI, Hu J, Looso M, *et al*. Mapping the endothelial cell S-sulfhydrome highlights the crucial role of integrin sulfhydration in vascular function. *Circulation*. 2021;143(9):935-948.

46. Weichsel A, Gasdaska JR, Powis G, Montfort WR. Crystal structures of reduced, oxidized, and mutated human thioredoxins: evidence for a regulatory homodimer. *Structure*. 1996;4(6):735-751.

47. Wang J, Wang W, Li S, *et al*. Hydrogen sulfide as a potential target in preventing spermatogenic failure and testicular dysfunction. *Antioxid Redox Signal*. 2018;28(16):1447-1462.

48. Estienne A, Portela VM, Choi Y, *et al*. The endogenous hydrogen sulfide generating system regulates ovulation. *Free Radic Biol Med*. 2019;138:43-52.

49. Ning N, Zhu J, Du Y, Gao X, Liu C, Li J. Dysregulation of hydrogen sulphide metabolism impairs oviductal transport of embryos. *Nat Commun*. 2014;5(1):4107.

50. Nuno-Ayala M, Guillen N, Arnal C, *et al*. Cystathionine β-synthase deficiency causes infertility by impairing decidualization and gene expression networks in uterus implantation sites. *Physiol Genomics*. 2012;44(14):702-716.

51. You X, Chen Z, Zhao H, *et al*. Endogenous hydrogen sulfide contributes to uterine quiescence during pregnancy. *Reproduction*. 2017;153(5):535-543.

52. Wang B, Xu T, Li Y, *et al*. Trophoblast H$_2$S maintains early pregnancy via regulating maternal-fetal interface immune hemostasis. *J Clin Endocrinol Metab*. 2020;105(12):e4275-e4289.

53. Osol G, Moore LG. Maternal uterine vascular remodeling during pregnancy. *Microcirculation*. 2014;21(1):38-47.

54. Jockusch BM, Isenberg G. Interaction of alpha-actinin and vinculin with actin: opposite effects on filament network formation. *Proc Natl Acad Sci U S A*. 1981;78(5):3005-3009.

55. Liu J, Wang Y, Goh WI, *et al*. Talin determines the nanoscale architecture of focal adhesions. *Proc Natl Acad Sci U S A*. 2015;112(35):E4864-E4873.

56. Sun Y, Huang Y, Yu W, *et al*. Sulfhydration-associated phosphodiesterase 5a dimerization mediates vasorelaxant effect of hydrogen sulfide. *Oncotarget*. 2017;8(19):31888-31900.

57. Untereiner AA, Olah G, Modis K, Hellmich MR, Szabo C. H$_2$S-induced S-sulfhydration of lactate dehydrogenase a (LDHA) stimulates cellular bioenergetics in hct116 colon cancer cells. *Biochem Pharmacol*. 2017;136(4):86-98.

58. Zhang H-H, Wang W, Feng L, *et al*. S-nitrosylation of cofilin-1 serves as a novel pathway for VEGF-stimulated endothelial cell migration. *J Cell Physiol*. 2015;230(2):406-417.

59. Zhang H-H, Lechuga TJ, Tith T, Wang W, Wing DA, Chen D-B. S-nitrosylation of cofilin-1 mediates estradiol-17beta-stimulated endothelial cytoskeleton remodeling. *Mol Endocrinol*. 2015;29(3):434-444.

60. Rosenfeld CR, Roy T, DeSpain K, Cox BE. Large-conductance Ca^{2+}-dependent K$^+$ channels regulate basal uteroplacental blood flow in ovine pregnancy. *J Soc Gynecol Investig*. 2005;12(6):402-408.

61. Rosenfeld CR, White RE, Roy T, Cox BE. Calcium-activated potassium channels and nitric oxide coregulate estrogen-induced vasodilation. *Am J Physiol Heart Circ Physiol*. 2000;279(1):H319-H328.

62. Xiao D, Longo LD, Zhang L. Role of K$_{ATP}$ and L-type Ca^{2+} channel activities in regulation of ovine uterine vascular contractility: effect of pregnancy and chronic hypoxia. *Am J Obstet Gynecol*. 2010;203(6):596.e6-596.e12.

63. Hu X-Q, Dasgupta C, Chen M, *et al*. Pregnancy reprograms large-conductance Ca^{2+}-activated K$^+$ channel in uterine arteries: roles of ten-eleven translocation methylcytosine dioxygenase 1-mediated active demethylation. *Hypertension*. 2017;69(6):1181-1191.

64. Fallahi S, Houck JA, Euser AG, Julian CG, Moore LG, Lorca RA. High altitude differentially modulates potassium channel-evoked vasodilatation in pregnant human myometrial arteries. *J Physiol*. 2022;600(24):5353-5364.

65. Tang G, Wu L, Liang W, Wang R. Direct stimulation of K$_{ATP}$ channels by exogenous and endogenous hydrogen sulfide in vascular smooth muscle cells. *Mol Pharmacol*. 2005;68(6):1757-1764.